ACS Catalysis

Research Article

pubs.acs.org/acscatalysis

Molecular Design of Non-Leloir Furanose-Transferring Enzymes from an α-L-Arabinofuranosidase: A Rationale for the Engineering of Evolved Transglycosylases

Bastien Bissaro,[†,‡,§] Julien Durand,[†,‡,§] Xevi Biarnés,[∥] Antoni Planas,[∥] Pierre Monsan,[†,‡,§,⊥] Michael J. O'Donohue,[*,†,‡,§] and Régis Fauré[*,†,‡,§]

[†]Université de Toulouse; INSA, UPS, INP; LISBP, 135 Avenue de Rangueil, F-31077 Toulouse, France

[‡]INRA, UMR792, Ingénierie des Systèmes Biologiques et des Procédés, F-31400 Toulouse, France

[§]CNRS, UMR5504, F-31400 Toulouse, France

[∥]Laboratory of Biochemistry, Institut Químic de Sarrià, Universitat Ramon Llull, Via Augusta, 08017 Barcelona, Spain

[⊥]Toulouse White Biotechnology, UMS INRA/INSA 1337, UMS CNRS/INSA 3582, 3 Rue des Satellites, 31400 Toulouse, France

Supporting Information

ABSTRACT: The vast biodiversity of glycoside hydrolases (GHs) constitutes a reservoir of readily available carbohydrate-acting enzymes that employ simple substrates and hold the potential to perform highly stereopecific and regioselective glycosynthetic reactions. However, most GHs preferentially hydrolyze glycosidic bonds and are thus characterized by a hydrolysis/transglycosylation partition in favor of hydrolysis. Unfortunately, current knowledge is insufficient to rationally modify this partition, specifically mutating key molecular determinants to tip the balance toward transglycosylation. In this study, in the absence of precise knowledge concerning the hydrolysis/transglycosylation partition in a hydrolytic GH51 α-L-arabinofuranosidase, we describe how an iterative protein engineering approach has been used to create the first "non-Leloir" transarabinofuranosylases. In the first step, random mutagenesis yielded a point mutation (R69H) at a position that is highly conserved in clan GH-A. Characterization of R69H revealed that this enzyme displays high transglycosylation activity but severely reduced (61-fold) activity on *p*NP-α-L-arabinofuranoside. Upon recombination of R69H with other point mutations selected using semirational or *in silico* approaches, transfer rates close to 100% and transarabinofuranosylation yields of the main (1→2)-linked oligosaccharide product of 80% (vs 11% for the wild-type) were obtained. Combining data presented here with knowledge drawn from the literature, we suggest that the creation of non-Leloir transglycosylases necessarily involves the destabilization of the highly developed transition states that characterize the predominantly hydrolytic *exo*-acting GHs; this is an efficient way to prevent ubiquitous water molecules from performing the deglycosylation step.

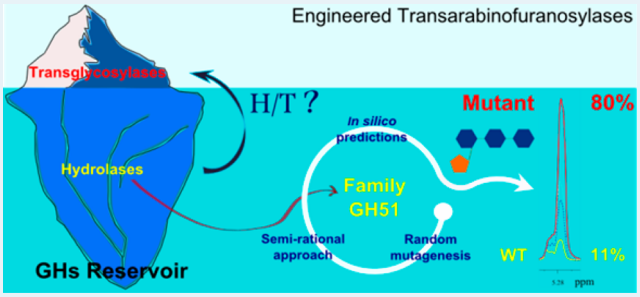

KEYWORDS: *biocatalysis, transglycosylation, molecular evolution, glycoside hydrolase, enzyme mechanism, pentose-based oligosaccharides*

INTRODUCTION

Considering the importance of carbohydrates in biological processes (i.e., in molecular recognition, the storage of energy, and also for structural purposes), the improvement and widening of our ability to synthesize glycosidic motifs and glycoconjugates is of the utmost importance. In this respect, chemo-enzymatic approaches are proving to be highly useful alternatives to purely chemical methods, although these have so far focused mainly on hexopyranoses, with furanoses being left aside, despite the fact that the synthesis of furanosides using conventional methods has often proved to be quite challenging.[1,2]

Carbohydrate active enzymes (CAZymes), such as glycosyltransferases (GTs) and so-called retaining glycoside hydrolases (r-GHs), are the workhorses of chemo-enzymatic approaches for the synthesis of complex carbohydrates.[3−6] In the case of GTs, the vast majority is designated as sugar nucleotide-dependent (Leloir) enzymes, whereas r-GHs that predominantly catalyze glycosynthetic reactions have often been referred to as non-Leloir transglycosylases (or TGs).

Regarding GHs, these are potentially very attractive for chemo-enzymatic strategies, because they are highly abundant, display a wide range of substrate specificities and often employ readily accessible, simple activated glycosides as donor compounds. The synthetic capability of r-GHs resides in their

Received: May 6, 2015
Revised: June 12, 2015
Published: June 15, 2015

DOI: 10.1021/acscatal.5b00949
ACS Catal. 2015, 5, 4598−4611

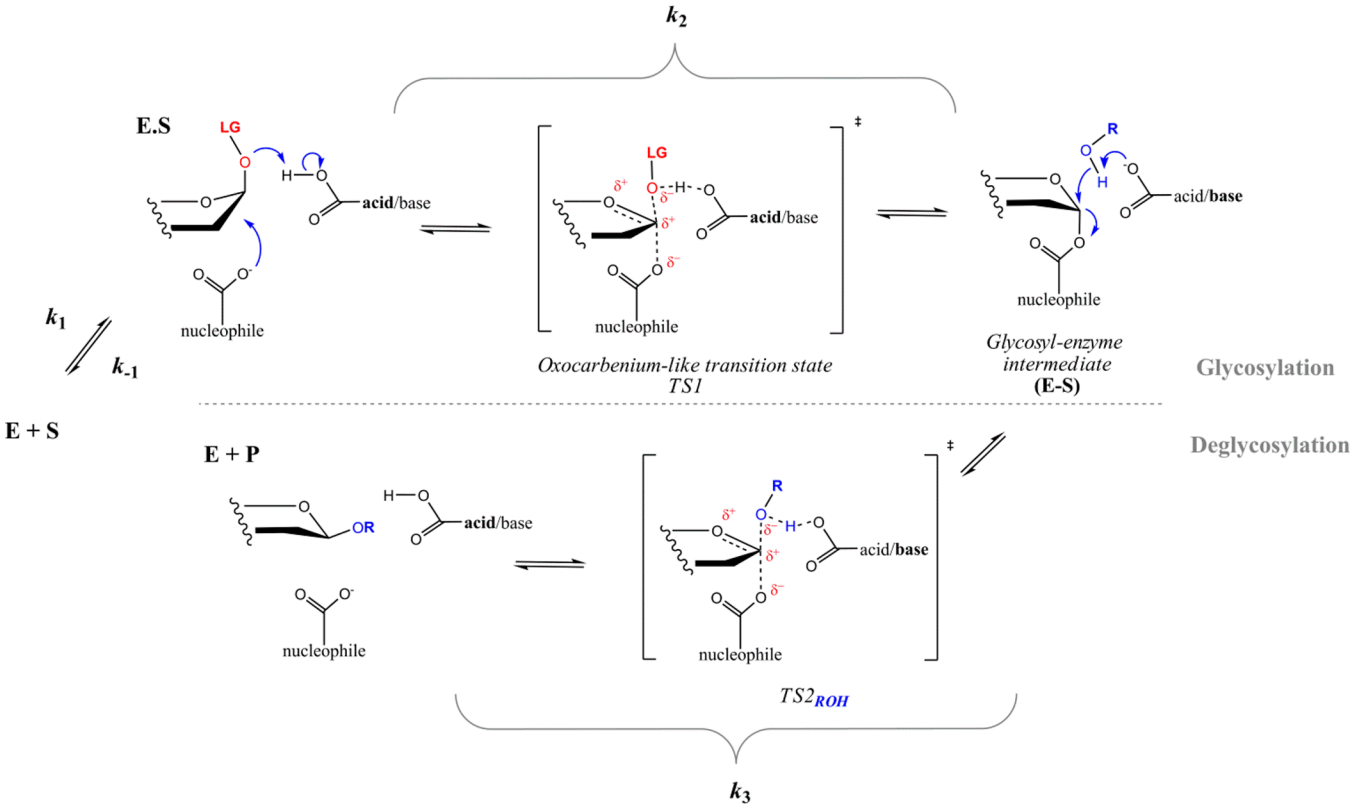

Figure 1. Two-step displacement mechanism of retaining GHs. Along the reaction mechanism, a Michaelis complex (E.S) is formed between the enzyme and the donor substrate allowing a nucleophilic attack of the catalytic nucleophile residue onto the anomeric carbon, combined with a protonation of the interglycosidic oxygen by the catalytic acid/base residue, leading to a release of the leaving group (LG) and formation of the covalent glycosyl-enzyme intermediate (E-S). This step is so-called the glycosylation step. The donor LG can be either an activated group (e.g., *p*NP) or a sugar (e.g., fructose for glucansucrases). Regarding the second step, denoted as deglycosylation step, the covalent glycosyl-enzyme intermediate can be either attacked by a water molecule (hydrolysis, R = H) or an external hydroxylated acceptor (transglycosylation, R = sugar, alkyl chain, etc.), which are activated by the deprotonated form of the acid/base catalytic residue. In the case of secondary hydrolysis, the transglycosylation product becomes a donor substrate with subsequent deglycosylation step involving water as acceptor. In this study, the donor substrate is *p*NP-α-L-Ara*f*, and the acceptor is xylotriose (Figure S1).

double-displacement mechanism, the outcome of which can be either hydrolysis or transglycosylation, the latter being dependent on the relative availability and the recognition of acceptors other than water in the reaction medium (Figure 1).[7] Nevertheless, most r-GHs principally display hydrolytic activity in aqueous medium, and only a minority of r-GHs can be described as TGs. During reactions catalyzed by TGs, the covalent glycosyl-enzyme intermediate is most readily deglycosylated by incoming sugar acceptors rather than water molecules, even in reaction media displaying high water activity, to the extent that the formation of glycosidic bonds is dominant and hydrolysis is low or even undetectable. Intriguingly, TGs are scattered among several CAZy GH families[8] (e.g., XET from GH16, amylosucrases from GH13, trans-sialidases from GH33; www.cazy.org and www.cazypedia.org), although no non-Leloir transfuranosylases have been described to date. Significantly, TGs are very frequently highly homologous to their hydrolytic family counterparts (e.g., amylosucrases/amylases from GH13). The implication of this observation is that the outcome of catalysis (i.e., hydrolysis or transglycosylation) is not determined by any single active site topology or protein 3-D structure but is probably associated with a range of more subtle molecular features.[9]

The quest to understand the underlying molecular determinants of the hydrolysis/transglycosylation (H/T) partition in r-GHs has challenged researchers for at least 20 years and has given rise to numerous hypotheses that are mostly only applicable to single GH families and fail to answer the fundamental question of how TGs perform glycosynthesis in environments dominated by water.[10−14] Indeed, only very recently has a more integrated approach been used to review current literature and provide more generic understanding of the H/T partition in r-GHs.[9]

Apart from the glycosynthase strategy[15,16] there are no clear-cut protein engineering guidelines to convert a hydrolytic r-GH into a TG (using nonfluorinated activated simple substrates), which led us in the present study to adopt a hybrid approach to engineer the hydrolytic GH51 α-L-arabinofuranosidase from *Thermobacillus xylanyliticus* (*Tx*Abf). For over a decade, this enzyme has been the subject of many studies that have not only characterized the ability of *Tx*Abf to hydrolyze bonds linking α-L-arabinofuranosyl (α-L-Ara*f*) moieties to D-xylopyranosyl (D-Xyl*p*) units in arabinoxylans and arabinoxylo-oligosaccharides (AXOS) of plant origin,[17] but these studies have also characterized its ability to perform transglycosylation. In several studies, we have shown how, in the presence of appropriate sugar or alcohol acceptors, the H/T partition can be driven toward transglycosylation, allowing the synthesis of a variety of furanose-based compounds, including L-arabino- and D-galactofuranosides.[18,19] Moreover, in recent work using *in vitro* random mutagenesis, we managed to tip the H/T balance further toward

DOI: 10.1021/acscatal.5b00949
ACS Catal. 2015, 5, 4598−4611

transglycosylation, creating novel glycosynthetic tools for the synthesis of complex furanoside-based structures that would be difficult to access using conventional synthetic chemistry.[20,21]

In the present study, we have pursued our efforts to engineer *Tx*Abf, this time combining our previously acquired knowledge to develop a hybrid engineering approach that has relied on random mutagenesis, site-saturation mutagenesis at previously identified hot-spots, and site-directed mutagenesis driven by *in silico* predictions. In this stepwise manner, we have succeeded in creating what can only be described as the very first non-Leloir transarabinofuranosylases, the biochemical characteristics of which are thoroughly described herein.

EXPERIMENTAL SECTION

Substrates and Chemicals. Unless otherwise stated, routine experimental work was performed using chemicals purchased from Sigma-Aldrich (Illkirch, France) and molecular biology reagents purchased from New England Biolabs (Evry, France). The substrate, 4-nitrophenyl α-L-arabinofuranoside (*p*NP-α-L-Ara*f*), was purchased from CarboSynth (Compton, U.K.) and xylotriose and XOS were purchased from Wako Chemicals GmbH (Neuss, Germany). Regarding other aryl α-L-arabinofuranosides used in this study, these were synthesized in-house using a modified version (Supporting Information) of a previously described synthetic route.[22]

Mutagenesis, Protein Expression, and Purification. *Site-Directed Mutagenesis.* The plasmid pET24-*Tx*Abf (the original pET vector was from Novagen, Fontenay-sous-Bois, France) was used as template DNA for *in vitro* mutagenesis using the QuikChange Site-Directed Mutagenesis kit (Agilent, Courtaboeuf, France), following the manufacturer's instructions. For recombination of mutations R69H, L352M, and G179F, the following primers (5′-3′) were employed (underlined codon and mutated base in bold):

R69H TCCGGTCCTC**CAC**TGGCCGGGCG
G179F GGCAACGAGAACTGG**TTC**TGCGGCGGC-AACAT
L352M CAGCTCGTCAACGTG**ATG**CAATCCGTCATCC

The successful introduction of mutations was confirmed by DNA sequencing (GATC Biotech, Mulhouse, France).

Large-Scale Enzyme Expression and Purification. To produce larger batches of wild-type and mutated recombinant *Tx*Abf, protein expression and purification were performed as previously described.[23]

Creation and Screening of Random Mutant Libraries. Design of Random Libraries. A randomly mutated gene library was constructed using pET24-*Tx*Abf-L352M as DNA template. For mutagenesis, the GeneMorph II Random Mutagenesis kit (Agilent) was employed following the suppliers recommendations. To generate optimal genetic diversity, three separate reactions were performed (50 μL each) in which the quantities of pET24-*Tx*Abf-L352M template DNA differed (50, 100, and 150 ng), but the amounts of dNTP mix (800 μM), primers mix (250 ng.μL^{-1} each), and Mutazyme II DNA polymerase (2.5 IU) were identical. The reactions were performed using a PCR thermocycler and the following protocol: one initial denaturing step at 95 °C for 2 min, followed by 25 cycles at 95 °C for 1 min, 55 °C for 1 min, 72 °C for 2 min, and a final elongation step at 72 °C for 10 min. For the PCR reactions, the sequences of the forward and reverse primers were 5′-GGAATTCCATATGAACGTGGCAAGCCGGGTAGTCG-3′ and 5′-CGATGGCCCACTACGTGAACCATC-3′, respectively. The forward primer contains a *Nde*I restriction site, and the reverse primer anneals to a sequence within the pET24 vector. Accordingly, the size of the amplicon was 1933 bp, representing the target *Tx*Abf-encoding sequence (1490 bp), associated with a part of the pET24 vector (433 bp). After purification using a DNA clean and concentrator kit (Zymo Research, USA), the amplicon was digested using *Nde*I (20 IU) and *Hind*III (20 IU) at 37 °C for 4 h in a buffered (1 X Neb2 buffer) reaction (50 μL). Afterward, the reaction was stopped by heating at 65 °C for 20 min, and an aliquot (20 IU) of *Dpn*I was added. Following further incubation at 37 °C for 1 h, the DNA fragments were purified and eluted in 10 μL of ddH_2O (Zymo Research kit). The resulting purified, mutated *Tx*Abf-encoding sequence was then ligated with *Hind*III/*Nde*I-digested pET-24 vector. To achieve this, five separate ligation reactions (15 μL each) were prepared in PCR tubes, each containing 55 ng of mutated *Tx*Abf-encoding DNA and 66 ng of linearized pET24 DNA (i.e., a 3:1 molar ratio), 1.5 μL of T4 DNA ligase buffer (10X), and 1 μL of T4 DNA ligase (400 IU). The reactions were incubated for 12 h at 16 °C and then 2 μL aliquots were used to transform aliquots (50 μL) of chemically competent *E. coli* Top10 cells. Overall, 24 transformation reactions were performed, after which the bacteria were spread onto LB-agar Petri dishes containing kanamycin (40 μg.mL^{-1}). Colonies were allowed to develop for 14 h at 30 °C before being suspended in 500 μL of liquid LB medium containing kanamycin, which were added to the surface of each plate surface. After recovery, the various cell suspensions were pooled, and the total volume was centrifuged (5000*g*, 10 min), providing a single cell pellet which was used to prepare purified plasmid DNA. This DNA sample constituted the L352M-based random library, which was stored at −20 °C until further use.

Screening. For library screening, 10 ng of the plasmid library DNA stock were used to transform chemically competent *E. coli* BL21 DE3 star cells, which were then grown at 37 °C for 12 h on a nitrocellulose membrane (0.45 μm, 20 × 20 cm) placed on selective LB agar medium contained within a Q-tray, thus allowing the development of small colonies (Ø < 0.5 mm). Likewise, eight Q-Trays were prepared, representing approximately 40 000 clones. Once colonies were formed, the nitrocellulose membranes were transferred onto selective, buffered (sodium phosphate buffer 100 mM, pH 7.0, agar 15 g·L^{-1}) minimal medium, containing IPTG (0.4 mM) and 5-bromo-4-chloro-3-indolyl α-L-arabinofuranoside, X-α-L-Ara*f* (0.1 mM final concentration, initially solubilized in DMSO), and incubated for 2 h at 30 °C. In parallel, a control membrane was prepared on which only colonies expressing the parental L352M variant were present. After 2 h, all membranes were examined, and colonies (∼400) displaying a pale blue color were selected and transferred into four 96-well microtiter plates containing 200 μL of LB-kanamycin (40 μg.mL^{-1}). Plates were incubated overnight at 30 °C with shaking (700 rpm), after which an aliquot (100 μL) was removed from each well and combined with a glycerol solution (25%, v/v final concentration) to create library backups. The backups were archived at −80 °C, and the remaining cell cultures were used to prepare cell-free lysates.

Preparation of Cell-Free Lysates of Library Clones. Using the previous microtiter cultures of the selected library clones to inoculate fresh LB-kanamycin medium (500 μL) in 96-deepwell (2 mL/well) microtiter plates, precultures were prepared and grown overnight (30 °C, 700 rpm). Afterward, 100 μL of each preculture was used to inoculate 900 μL aliquots of fresh

DOI: 10.1021/acscatal.5b00949
ACS Catal. 2015, 5, 4598−4611

LB-kanamycin contained in wells of 96-well deepwell microtiter plates. These cultures were incubated at 37 °C and 700 rpm during 2 h, and then IPTG (0.5 mM final) was added and incubation was pursued (18 h incubation at 18 °C and 700 rpm). Subsequently, cells from each culture were recovered using centrifugation (2250*g*, 20 min) and suspended in 300 μL of Tris-HCl buffer (20 mM, pH 8.0) containing lysozyme (0.5 mg.mL^{-1}), and incubated 1 h at 30 °C, followed by freezing overnight at −80 °C. After thawing (30 °C, 30 min), the cell suspensions were heat-treated (75 °C, 30 min) and clarified lysates were prepared by centrifugation (2250*g*, 50 min, 4 °C). Finally, lysates were transferred into fresh 96-well microtiter plates and stored at 4 °C.

Secondary Screening of Selected Clones. The 400 cleared lysates representing individual library clones were used to perform kinetic analyses using an automated protocol that provided the means to simultaneously perform 96 analyses. Likewise, it was possible to compare the activities of individual lysates in the presence and absence of acceptor, and thus derive an activity ratio (R), which was equal to $Vi_{(donor+acceptor)}/Vi_{(donor)}$. Using a liquid handling system (Genesis RSP 200, Tecan), reactions were prepared in wells of 96-well polypropylene PCR microtiter plates (Corning, Sigma-Aldrich). The basic reaction mixture used to determine $Vi_{(donor)}$ values was composed of 135 μL substrate solution (15 mM *p*NP-α-L-Ara*f* in 50 mM sodium phosphate, pH 7.0) and 15 μL (10% of final volume) of lysate. To determine the value of $Vi_{(donor+acceptor)}$, the reaction was performed as before, but 10 mM xylotriose (i.e., acceptor) was added to the reaction mixture. To perform reactions, the substrate solution (with or without acceptor) was first incubated at 45 °C for 15 min in a Peltier heating device, before initiating the reaction through the addition of lysates. Once initiated, the progression of reactions was monitored by removing 20 μL aliquots every 6 min (4 points in total, each reaction lasting 24 min). These were immediately combined with 180 μL of 1 M Na_2CO_3, and absorbance (405 nm) was determined. Using a simple, purpose-designed Excel macro, the activity (IU/mL) of the different clarified lysates was calculated in the presence and absence of acceptor, and activity ratios were derived for each one. The relative mean error of this method was 4% for any single lysate. For each microtiter plate, standard deviations (σ) were calculated, and 1.96 σ was represented, which is the approximate value for the 97.5 percentile point of a normal distribution.

N216X Site Saturation Library Design and Screening. A site saturation mutagenesis experiment of the type NNS was performed at position N216. To achieve this, the *Tx*Abf-encoding sequence was first mutated at position 216, introducing a stop codon (TAG) using QuickChange II Site-Directed Mutagenesis kit (Stratagene, Amsterdam, The Netherlands) and an appropriate primer pair (forward primer is shown below). This mutated DNA was then used as a template for NNS mutagenesis, which was performed using the same mutagenesis kit and appropriate primers (forward primer is shown below).

N216Stop TGCGTGCGGCGCG**TAG**ACGGCCGAC-TACCA

N216X TGCGTGCGGCGCG**NNS**ACGGCCGAC-TACCA

Taking into account the theoretical size of the NNS library, it was considered that the selection and screening of 96 clones would cover 95% of the diversity.[24] Therefore, 96 randomly picked *E. coli* BL21(DE3) colonies were used for enzyme production in microtiter plate format as previously described. Afterward, the 96 clarified lysates were submitted to automated kinetic analyses in the absence and presence of a mixture of xylo-oligosaccharides as acceptor as described above. One mutant revealed an increased ratio (R = 1) relative to *Tx*Abf (R = 0.4) and was identified as N216W after sequencing.

***In Silico* Screening of *Tx*Abf against Xylotriose.** The binding affinity of a library of *Tx*Abf mutants for xylotriose was screened *in silico* using a model of the 3D structure of the covalent β-L-Ara*f*-*Tx*Abf intermediate involving a xylotriosyl moiety (Supporting Information). Sequence variations were allowed only at those sequence positions located within 10 Å of *Tx*Abf subsites +2′, +1, +2, and +3.

Determination of Kinetic Parameters. *Hydrolytic Behavior.* The kinetic parameters describing hydrolysis catalyzed by wild-type or mutant *Tx*Abf were determined using a continuous assay in which the release of different phenolates was monitored using either an Eon spectrophotometer (BioTek), or in the case of PhOH, a Cary 100 Bio UV−vis spectrophotometer (Agilent). Reactions were performed at 45 °C (a choice of temperature that translates a compromise between enzyme activity and stability) in wells of microtiter plates containing 50 mM sodium phosphate buffer, pH 7.0, substrate, 0.1 mg·ml^{-1} BSA and enzyme, in a final reaction volume of 200 μL. Taking into account the fact that the substrates were initially dissolved in DMSO, the final DMSO concentration in reactions was always less than 2% (v/v). To perform reactions, the buffered substrate mixture (180 μL) contained in microtiter plate wells was equilibrated at 45 °C for 5 min; then 20 μL of an appropriately diluted enzyme solution was added, and the release of LG was monitored at 400 (for *p*NP, 3-NP and 3,4-dNP) or 425 nm (for NCP). For reactions involving Ph-α-L-Ara*f*, these were performed in a similar way, but in a final volume of 500 μL in quartz cuvettes, and the release of phenol was monitored at 280 nm. Control reactions containing all the reactants except the enzyme were used to correct for slight spontaneous hydrolysis of the substrates, which was observed in the case of 3,4-dNP-α-L-Ara*f* and NCP-α-L-Ara*f*. Furthermore, standard curves of substrates were prepared to correct for absorbance of the phenyl group in its bound form (i.e., Ph-α-L-Ara*f*). Moreover, a standard solution of *p*NP was used to compare the difference in the response coefficients of the Eon and Cary spectrophotometers. This proved to be less than 6%. Initial reaction rates were determined from the linear regions of time-dependent plots, which corresponded to 5−15% consumption of the substrate. Substrate concentrations were typically varied from 0.1 to 18 mM. One unit (IU) of enzyme specific activity corresponds to the amount of enzyme releasing 1 μmol of LG per minute. Steady-state kinetic parameters were determined using nonlinear regression functions embedded in the SigmaPlot 11.0 software (Systat software Inc., Ritme, Paris, France). Three models were employed, including the classical Michaelis−Menten model, inhibition by excess substrate model, and a modified Michaelis−Menten that accounts for donor-induced activation through self-condensation. Steady-state kinetic parameters were then analyzed using the Brønsted correlation according to eqs 1 and 2.

$$\log(k_{cat}/K_M) = \beta_{LG1}\cdot pK_a^{LG} + c_1 \quad (1)$$

$$\log(k_{cat}) = \beta_{LG2}\cdot pK_a^{LG} + c_2 \quad (2)$$

To measure solvent kinetic isotope effects (sKIE), reactions were performed at 45 °C, pH 7.0 as described earlier, using NCP-α-L-Ara*f* in D_2O. In reactions involving either R69H or R69H-L352M, substrate concentration was 2 mM, whereas those

DOI: 10.1021/acscatal.5b00949
ACS Catal. 2015, 5, 4598−4611

involving *Tx*Abf and L352M had a substrate concentration of 5 mM. The D_2O content of the reaction was varied (35, 50, 65, 80, and 100%) by adding appropriate amounts of H_2O to reach 180 μL. The enzymes were prediluted in D_2O, and 20 μL of enzyme solution was used in each reaction, providing a final volume of 200 μL.

To determine the effect of pH on enzymes, an analysis of k_{cat}/K_M was performed, using the previously described protocols to determine in duplicate the values of k_{cat} and K_M. In these reactions, the concentration of *p*NP-α-L-Ara*f* was varied between 0.15 and 18 mM, and pH was varied in the range of 4.5 to 8.7 using 100 mM citrate-sodium phosphate buffer (pH 4.5−7.0) and 100 mM sodium phosphate buffer (7.0−8.7), with a common point being measured in both buffers at pH 7.0 for each enzyme and each substrate concentration. Control experiments in the absence of enzyme were performed at each pH value in order to monitor any spontaneous hydrolysis of the substrate during the duration of the reaction (30 min). Lastly, the ratio k_{cat}/K_M was plotted as a function of pH and fitted to a bell-shaped activity profile according to eq 3.[25] This analysis provided the apparent pK_a values corresponding to the nucleophile (pK_{a1}) and the acid/base (pK_{a2}) catalytic amino acids, which were determined by nonlinear least-squares fitting using Microsoft Excel 2010. When a "tail" was observed on the basic side of the pH-dependent profile, eq 4 was employed.[26]

$$\frac{k_{cat}}{K_M} = \left(\frac{k_{cat}}{K_M}\right)\max \cdot \left(\frac{1}{1 + 10^{pK_1 - pH} + 10^{pH - pK_2}}\right) \quad (3)$$

$$\frac{k_{cat}}{K_M} = \frac{\left(\frac{k_{cat}}{K_M}\right)_1 + \left(\frac{k_{cat}}{K_M}\right)_2 \cdot 10^{(pH - pK_2)}}{1 + 10^{pK_1 - pH} + 10^{pH - pK_2} \cdot (1 + 10^{pH - pK_3})} \quad (4)$$

Acceptor Impact on Global Activity. To measure the influence of acceptor substrate concentration on *p*NP release, reactions were performed in which the donor (*p*NP-α-L-Ara*f*) concentration was held constant (5 mM) while the acceptor (xylotriose) concentration was varied. When acceptor-mediated inhibition was observed, a mixed model described by eq 5 was employed to fit experimental data, whereas eq 6 was used when acceptor-mediated activation occurred.

$$\frac{V_i}{V_{max}} = \frac{(1/\alpha') \cdot S}{(\alpha/\alpha') \cdot K_M + S} \quad \text{with } \alpha' = 1 + \frac{[I]}{K_i'} \text{ and } \alpha = 1 + \frac{[I]}{K_i} \quad (5)$$

$$= \frac{V_{max} \cdot [Donor] \cdot [Acceptor]}{K_M^{donor} \cdot [Acceptor] + [Donor] \cdot [Acceptor] + K_M^{acceptor} \cdot [Donor]} \quad (6)$$

Monitoring Transglycosylation. *Time Course of NMR Monitoring.* To monitor reactions by collecting ^{1}H NMR spectra on a Bruker Avance 500 spectrometer, enzyme solutions were first prepared by 10-fold dilution in D_2O (99.90%) and then concentrated on an Amicon Ultra filter (regenerated cellulose 10 kDa, Millipore), performing the operation twice. Afterward, reactions were performed at 45 °C in NMR tubes containing 600 μL of buffered D_2O, *p*NP-α-L-Ara*f* as donor and xylotriose as acceptor, at a ratio of 1:2 (15 and 30 mM, respectively). To obtain a pD value of 5.8, deuterated acetate (Euriso-Top, France) buffer was employed, while pD 7.1 was achieved using a deuterated sodium phosphate buffer, which was prepared by dissolving sodium phosphate in D_2O, followed by lyophilization. This two-step protocol was repeated three times to obtain sufficient deuteration. Values of pD were measured by determining pH using a glass pH electrode and then applying the equation pD = $pH_{electrode}$ + 0.41.[27] To initiate reactions, an aliquot of enzyme solution (never exceeding 5% of total reaction volume) was added to the reaction, the quantity of enzyme (18 nM for *Tx*Abf and N216W, 50 nM for G179F and L352M, and 2000 nM for all R69H-containing mutants) being adjusted to suit the 8−12 h reaction time frame. ^{1}H NMR spectra were accumulated semicontinuously, collecting a series of 5.52 min scans (i.e., 32 scans) with 6 s delays between scans. Each ^{1}H NMR spectrum was acquired using an excitation flip angle of 30° at a radiofrequency field of 29.7 kHz, and the reference residual water signal, calibrated at δ = 4.55 ppm at 45 °C,[28] was presaturated during the repetition delay (with a radiofrequency field of 21 Hz). The following acquisition parameters were used: relaxation delay (6 s), dummy scans (4). The actual duration of the reaction was dependent on the enzyme used. Prior to enzyme addition, an initial ^{1}H NMR spectrum was acquired, which provided starting point integrals that were subsequently corrected using a dilution factor that accounted for the minor dilution provoked by the addition of the enzyme solution.

NMR Kinetics Analysis. Data were processed as previously described.[23] Briefly, the time-dependent evolution of donor (*p*NP-α-L-Ara*f*) and acceptor (xylotriose) concentrations was quantified by integrating the relevant anomeric proton signals. Molar balances, based on acceptor and donor consumption, were used to convert the transglycosylation product signal integral into concentration, and to evaluate concentrations of hydrolysis products, respectively. From this, the donor substrate conversion rate (X, in %) was calculated as the mean of three distinct signals: those of the *ortho* and *meta* aromatic protons (*p*NP) and that of the anomeric proton (L-Ara*f*), with X accounting for both reaction outcomes (i.e., hydrolysis and transglycosylation), and identifying self-condensation. For all time-course NMR kinetics, the absolute error mean value on X ranged from 1 to 3%. The transglycosylation yield, $Y_{(product)}$, was determined by relative integration of product anomeric proton signals, these being at 5.39, 5.32, and 5.27 ppm for XA^{3}X, A^{3}XX and A^{2}XX respectively.[29−34] Finally, $Y_{(product)}$ (%) was plotted against X (%) to provide the transfer rate (R_T) of the donor substrate to a given product (μmol of product/μmol of consumed substrate). Finally, initial rates were derived from the linear regions in which the variation of X was from 0 to 25% up to 0−40%, with root-mean-square deviations between 0.96 and 0.99.

Parameters To Evaluate the Effective Transition from Hydrolase to Transglycosidase. The activity ratio R (i.e., $Vi_{(donor+acceptor)}/Vi_{(donor)}$) putatively reflects the T/H partition (with Vi defined as the donor substrate consumption rate, which correlates with *p*NP release rate). However, to compare different enzymes that potentially display different activities, the transfer rate (R_T) of the donor substrate to a given product (μmol of product/μmol of consumed substrate) was obtained by plotting the yield of transglycosylation product(s) as a function of donor conversion. Conveniently, being independent of the duration of the reaction, R_T provides a way to compare different enzymes. Rho, which represents the apparent synthesis/hydrolysis rate, is equal to $|\nu_T/\nu_{HII}|$, with the apparent transglycosylation (ν_T, initial phase of the plot) and the secondary hydrolysis (ν_{HII}, after maximum yield) rates being derived from the time-course monitoring of transglycosylation product(s) yield.

RESULTS

Detection of Increased Transfuranosylation among Randomly Generated Mutants. An earlier random mutagenesis experiment performed on *Tx*Abf identified L352M among

DOI: 10.1021/acscatal.5b00949
ACS Catal. 2015, 5, 4598−4611

Table 1. Steady-State Kinetic Parameters on *p*NP-α-L-Ara*f* for L352M, R69H, and Mutants Thereof[a]

enzyme	pH_{opt}	SA_{max} (IU·mg^{-1})	k_{cat} (s^{-1})	K_M (mM)	k_{cat}/K_M (s^{-1}·mM^{-1})	Ns[b] (s^{-1}·mM^{-1})
*Tx*Abf	5.8	145	139	0.25	556.00	-
L352M	6.5	243	233	8.98	25.95	-
R69H	6.5	2.383	2.287	0.09	25.41	0.049
R69H-L352M	6.5	1.012	0.972	1.23	0.79	0.031
R69H-G179F-L352M	6.5	0.556	0.535	0.69	0.78	0.021
R69H-N216W-L352M	6.5	0.603	0.580	0.48	1.21	0.034

[a]All assays were carried out at 45 °C in sodium phosphate buffer (pH 7, 50 mM) in triplicates. Relative errors were inferior to 10%. [b]The Ns value corresponds to the nonspecific constant attributed to autocondensation reaction and was obtained according the following Michaelis−Menten modified model: $SA = SA_{max}\cdot[S]/(K_M + [S]) + Ns\cdot[S]$.

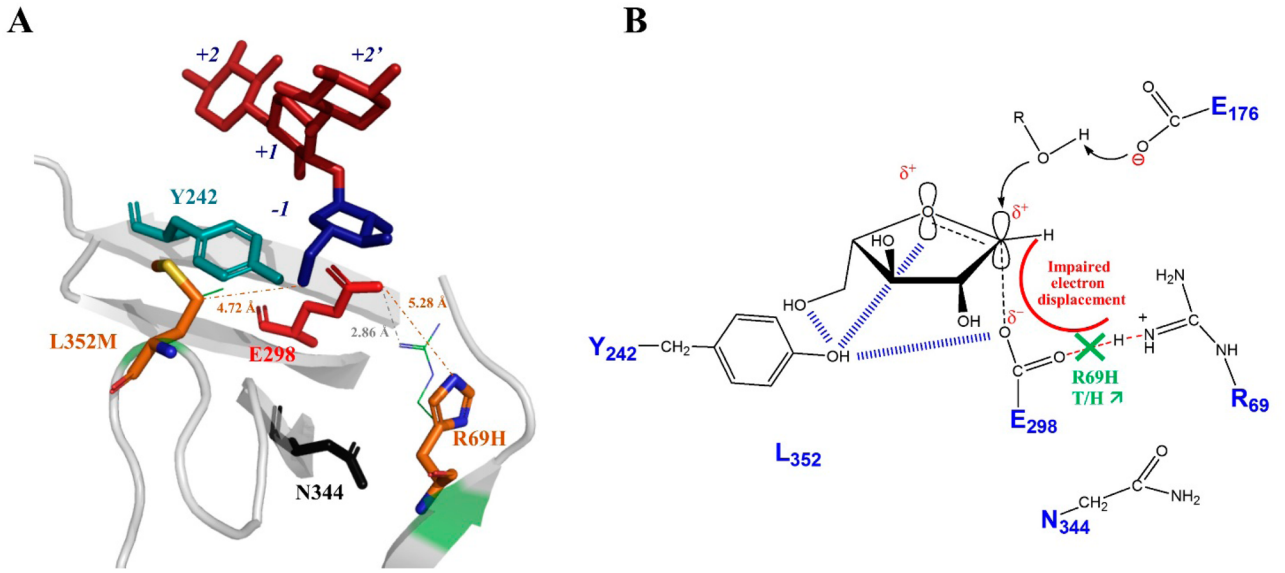

Figure 2. (A) Location of R69H and L352M within *Tx*Abf subsite −1 and (B) putative impact of the mutation R69H on the electronic displacement system during the establishment of the transition state at the deglycosylation step. R69 is at H-bond distance (2.86 Å) from the nucleophile catalyst E298, E176 playing the role of acid/base. Figure 2A was prepared using PyMOL Molecular Graphics System, v0.99 (Schrödinger).

several mutants that appeared to improve transglycosylation.[19] However, because the transglycosylation yield of L352M was still rather modest (approximately 18%), this mutant was used as a starting point for a new round of engineering. In the absence of clear-cut knowledge that would allow rational engineering, we chose to pursue the random approach and thus created a new randomly mutated library using *Tx*Abf-L352M as the parental DNA. Sequence analysis of 24 randomly selected clones from this library revealed a mean mutation rate of 3.2 amino acid mutations/kb (Figure S2) and screening of 40 000 library clones on solid medium containing the chromogenic substrate X-α-L-Ara*f* (Figure S3) allowed the selection of 368 pale blue colonies. Referring to the results of previous work,[20,35] it was considered that the latter probably represented a subset of hydrolytically impaired mutants, and thus a group of candidates for the identification of increased transglycosylation activity. Therefore, further *in vitro* screening was performed on these library clones in order to determine their relative activities on *p*NP-α-L-Ara*f*, in the presence or absence of the xylotriosyl acceptor (Figure S4). Overall, secondary screening revealed a ratio mean value (μ) for the activity ratio R of 0.86, implying that most clones displayed slight acceptor-mediated inhibition. Nevertheless, four clones lay outside of the 95% confidence interval ($R = \mu \pm 1.96\,\sigma$). One was the negative clone 123 (Figure S5), whereas three were positive clones (i.e., 165, 197, and 241), which formed a separate population that displayed more than 200% activity in the presence of xylotriose. Further investigation of these clones, using HPAEC-PAD to monitor the reactions, confirmed that the activity ratios of clones 165, 197, and 241 were significantly above the mean value (Figure S6). DNA sequencing of clones 165, 197, and 241 revealed that each of these contained the mutation R69H, although the overall genotype was different in each case (Table S1), thus providing a strong indication that R69H substitution was responsible for the measured phenotype. This conclusion was further supported by the examination of the molecular model of *Tx*Abf (PDB ID: 2VRQ), which revealed that R69 is located close (2.86 Å) to the catalytic nucleophile (Figure 2A).

Deconvolution and Recombination: Synergistic Effects between Donor and Acceptor Mutations. *Impact of R69H on the H/T Ratio.* To further investigate the consequences of the R69H mutation, this point mutation was introduced into the genetic backgrounds of both *Tx*Abf and the mutant L352M, thus creating mutant enzymes R69H and R69H-L352M respectively, and eliminating the extra substitution, V225M, present in clone 197. This was justified by the fact that V225 is located far from the active site (approximately 18 Å), is not very conserved (~31%) in family GH51, and is substituted at equivalent positions in other GH51 members by a whole variety of amino acids (excluding cysteine, phenylalanine, and tryptophan). Gratifyingly, subsequent analysis of the purified R69H-L352M enzyme confirmed the previous results obtained using the lysate

DOI: 10.1021/acscatal.5b00949
ACS Catal. 2015, 5, 4598−4611

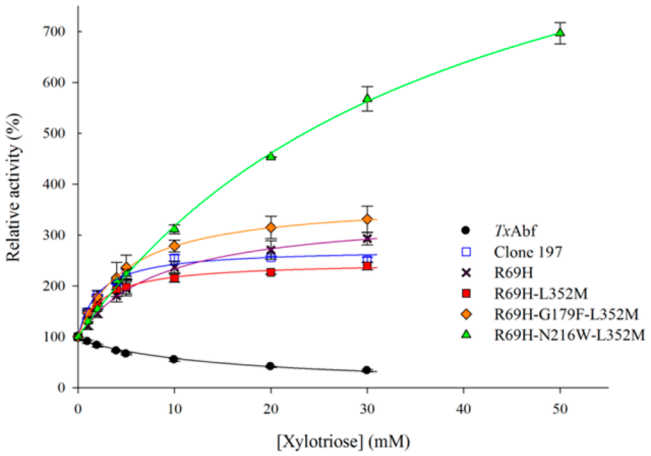

Figure 3. Analysis of the impact of xylotriose on global activity (*p*NP release) for *Tx*Abf, clone 197, R69H, R69H-L352M, R69H-G179F-L352M, and R69H-N216W-L352M. For the latter, an additional xylotriose concentration was tested (50 mM) because the plateau-phase was not reached. Assays were carried out in duplicate at 45 °C in sodium phosphate buffer (50 mM, pH 7) with *p*NP-*α*-L-Ara*f* as donor substrate (5 mM). Apparent K_i and K_i' values for xylotriose and *Tx*Abf are 15.0 and 15.6 mM. For R69H, R69H-L352M, R69H-G179F-L352M, and R69H-N216W-L352M mutants, apparent $K_M^{xylotriose}$ values for the acceptor are 8.6, 3.5, 5.9, and 45.5 mM.

of clone 197 and revealed that activity was increased up to 260% in the presence of xylotriose (Figure 3), unlike wild-type *Tx*Abf, which is inhibited (e.g., 30% of residual activity in the presence of 30 mM xylotriose). Factually, relative activity ratios were multiplied up to 7.2-fold (for R69H-L352M) compared to that of *Tx*Abf, suggesting that transglycosylation might be significantly reinforced. Furthermore, the analysis of purified R69H demonstrated that this mutation alone is adequate to radically alter this ratio.

Creation of Acceptor Subsite Mutations G179F (+1) and N216W (+2). To pursue the goal of creating a finely tuned transfuranosylase, two other positions were targeted for mutation. The first of these, G179 located in subsite +1, was pinpointed using an *in silico* screening approach (unpublished), which was used to identify point mutations that could potentially increase hydrophobicity at positive subsites and raise the affinity for the acceptor. When compared to other amino acid positions, a large number of substitutions at position G179 were predicted to modify the binding affinity of *Tx*Abf toward xylotriose (Figure S7). Therefore, position G179 was selected for mutation. Accordingly, the mutant G179F was found to display stronger xylotriose-mediated inhibition, implying that this mutant binds the acceptor molecule more tightly than the wild-type enzyme (Figure S8) and significantly improved transglycosylation yield and transfer rate (Table S2).

The second position targeted for mutation was N216, an amino acid located in subsite +2 that displays only partial conservation in family GH51 (25%, Table S3). Nevertheless, this residue stands out in *Tx*Abf as a good target for site-saturation mutagenesis, because inspection of the *in silico* model suggested that N216 is well-placed to influence the positioning of acceptor molecules.[36] Screening of the subsequent mutant library revealed one clone containing the mutation N216W, a substitution that is not found in any family GH51 members. Interestingly, compared to *Tx*Abf, this mutant was characterized by an almost total absence of inhibition in the presence of xylotriose (Figure S8), and further analysis revealed that it catalyzes the highly regioselective synthesis of (1→2)-linked products (Figure S9 and Table S2). Finally, using the mutants G179F and N216W, a combinatorial approach was adopted, constructing triple mutants R69H-G179F-L352M and R69H-N216W-L352M (Figure 4).

Kinetic Analyses of Mutants Combining R69H and L352M. Steady-state kinetic parameters were determined for the hydrolysis of *p*NP-*α*-L-Ara*f* catalyzed by the different mutants bearing the substitutions R69H and L352M (Table 1). Regarding the single mutants (i.e., those containing only R69H or L352M), both displayed significantly modified behavior. In the case of L352M, a 37-fold increase of the K_M value led to a 22-fold reduction in the k_{cat}/K_M value, indicative of a modification in the glycosylation step. The behavior of the R69H mutant was radically different to that of *Tx*Abf, because

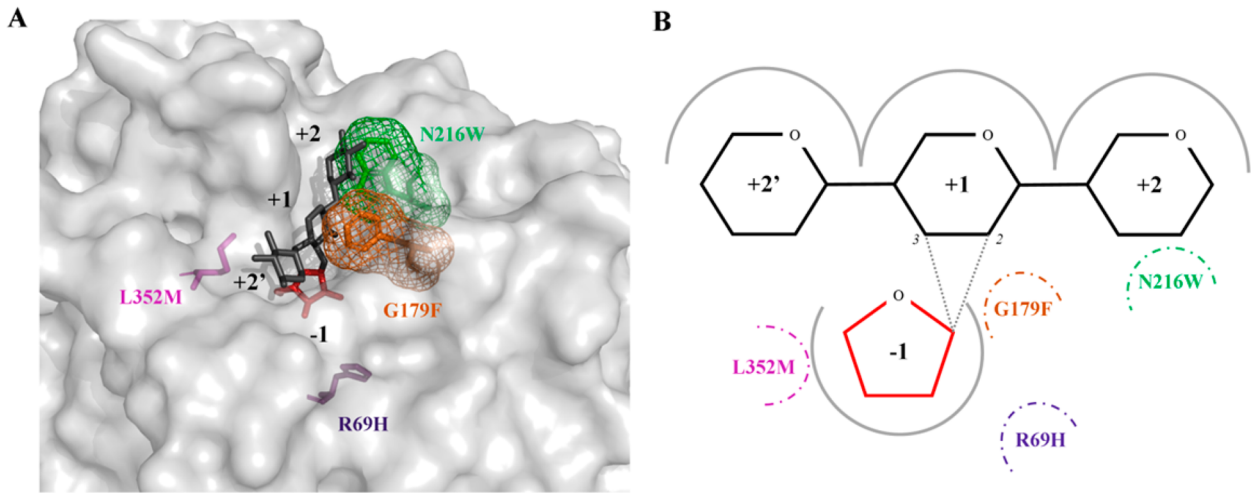

Figure 4. Location of the mutations in donor subsite −1 (L352M and R69H) and acceptor subsites +1 (G179F) or +2 (N216W). (A) 3D view of cocrystallized *Tx*Abf-XA^{3}XX (PDB ID: 2VRQ)[36] X-ray structure in which mutations were introduced via PyMOL Molecular Graphics System, v0.99 (Schrödinger). One can observe a steric clash between N216W and +2 D-Xyl*p* unit, explaining (1 → 3) linkage deletion by N216W mutant and putative stacking interactions between G179F and +1 D-Xyl*p* unit. (B) 2D-schematic representation of *Tx*Abf active site.

DOI: 10.1021/acscatal.5b00949
ACS Catal. 2015, 5, 4598−4611

the reaction was described by a biphasic profile (Figure S10). At *p*NP-*α*-L-Ara*f* concentrations below 5 mM, the reaction was described by the classical Michaelis−Menten model. However, at higher substrate concentrations, a linear relationship was observed, and overall, the rate of the reaction was severely reduced. Regarding the double mutant R69H-L352M and the triple mutants R69H-G179F-L352M and R69H-N216W-L352M, their behavior was highly similar to that of the single mutant R69H. All displayed severely reduced specific activities and biphasic reaction profiles.

Measurement of the Transglycosylation Activity of the Combinatorial Mutants. Contrary to *Tx*Abf, mutants R69H-L352M, R69H-G179F-L352M, and R69H-N216W-L352M revealed activation in the presence of xylotriose (Figure 3), fitting to eq 6 and providing apparent $K_M^{xylotriose}$ values of 3.5, 5.9, and 45.5 mM, respectively. This resulted for example in a 17.1-fold higher activity for R69H-N216W-L352 M compared to *Tx*Abf in the presence of 30 mM xylotriose (Table S4). Moreover, when xylotriose concentration was 50 mM, the relative activity of R69H-N216W-L352M attained 700% without reaching a plateau-phase. To pursue the characterization of the transfer ability of the different mutants, the synthesis of arabinoxylo-oligosaccharides (AXOS, see Fauré et al.[37] for a comprehensive description of AXOS nomenclature. Briefly, an unsubtituted D-Xyl*p* is designated X, whereas *α*-L-Ara*f*-(1→n)-*β*-D-Xyl*p* segment is named A^n with *n* corresponding to the *O*-position of the D-Xyl*p* unit involved in the linkage) was monitored by ^{1}H NMR using *p*NP-*α*-L-Ara*f* (15 mM) as donor and xylotriose (30 mM) as acceptor, and the results were displayed in two formats. The conversion-dependent plot (Figure 5A) constitutes the best way to compare the performance of mutants in the initial phase of the reaction, although plotting synthesis as a function of time (Figure 5B) provides a convenient method to evaluate the extent of secondary hydrolysis. Accordingly, results confirmed that the parental mutant L352M procured a 2-fold increase in transglycosylation yield compared to *Tx*Abf (Table S2) and displayed a significantly reduced level of secondary hydrolysis (Figure 5B). In the case of the other single mutant, R69H, the yield of A^{2}XX reached 31% (Table 2), but strong secondary hydrolysis at the end of the reaction led to the degradation of the product. Nevertheless, overall R69H displayed a 3.6-fold increase in the apparent synthesis/hydrolysis rate (Rho) of A^{2}XX (Table S5). Moreover, this single mutation led to a 4.3-fold increase in transfer rate (R_T) for A^{2}XX and a global R_T of 99% (XA^{3}X + A^{3}XX + A^{2}XX + XA^{2}X) in the initial phase of the reaction (Table S6), demonstrating that in this phase R69H confers strong transglycosylase character to *Tx*Abf. In comparison, the transglycosylation yields procured by the double mutant R69H-L352M, were slightly lower (27, 22 and 20%, for A^{2}XX, A^{3}XX and XA^{3}X respectively). However, the contribution of L352M was reflected in the higher R_T value (for A^{2}XX) and slower secondary hydrolysis. Overall, the combination of R69H and L352M produced a Rho value of 55, which constitutes a 26.9-fold increase compared to *Tx*Abf.

Analysis of the triple mutant, R69H-G179F-L352M, revealed that the presence of the mutation G179F led to postponed secondary hydrolysis, which had a beneficial effect on the maximum yield of the principal product A^{2}XX (49%) and on the yields of A^{3}XX and XA^{3}X (17 and 35%, respectively). In the case of R69H-N216W-L352M, high regioselectivity (1→2 linkage toward the nonreducing unit of xylotriose) and the alleviation of inhibition conferred by the N216W led to a dramatic increase in maximum yield (up to 79% compared to the approximate

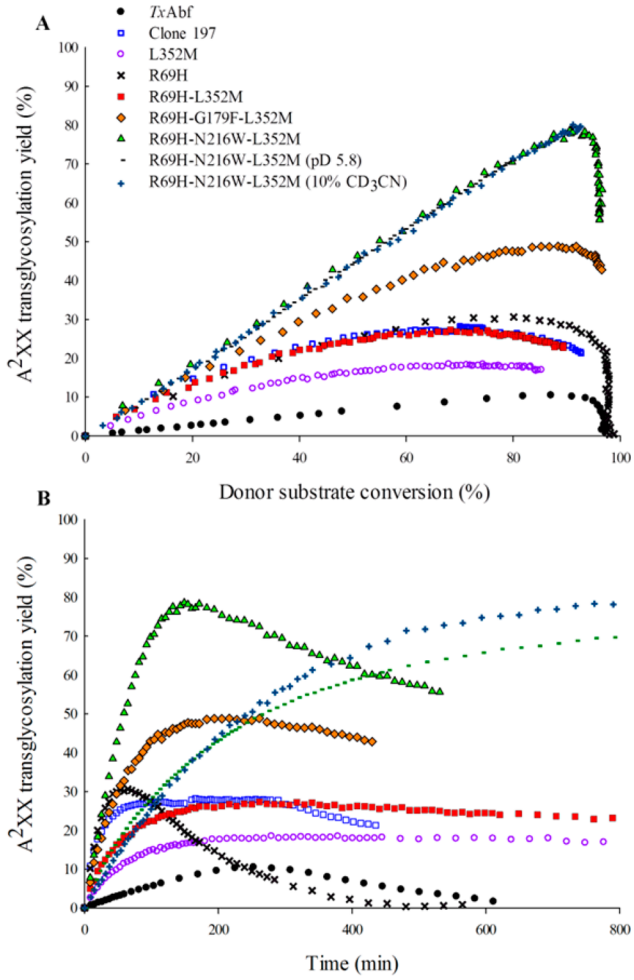

Figure 5. A^{2}XX major transglycosylation product evolution as a function of (A) donor conversion or (B) time for *Tx*Abf (pD 5.8), clone 197, L352M, R69H, R69H-L352M, R69H-G179F-L352M, and R69H-N216W-L352M. All assays were carried out at 45 °C in sodium phosphate buffer (25 mM, pD 7.0) or, when stated, in sodium acetate buffer (25 mM, pD 5.8), with *p*NP-*α*-L-Ara*f* as donor substrate (15 mM) and xylotriose as acceptor (30 mM), using 2 *μ*M of enzyme, except for *Tx*Abf and L352 M in which 18 and 50 nM were employed, respectively.

equimolar mixture of the different regioisomers obtained with the wild-type, Table 2) and R_T, which reached 90% for A^{2}XX. This is equivalent to a 6.9-fold increase of R_T compared to *Tx*Abf (Table S6). However, inevitably the generation of a high concentration of the transglycosylation product in the reaction mixture also led to strong secondary hydrolysis once the donor substrate had been consumed. Compared to R69H-L352M, this is consistent with a lower Rho value, which was nevertheless 7-fold higher than that measured for *Tx*Abf (Table S5). In a previous study,[23] it was revealed how a pH-dependent inhibition of *Tx*Abf could be used to block the degradation of transglycosylation products. Therefore, in the present work, this strategy was successfully employed in combination with the mutant R69H-N216W-L352M. Accordingly, by shifting the pH of the reaction from 7.0 to 5.8, it was possible to obtain A^{2}XX in yields >70%, without the inconvenience caused by secondary hydrolysis (Figure 5 and Table 2). It is noteworthy that the change in pH did not affect the transfer rate, indicating that the H/T partition is not pH-dependent for the mutant R69H-N216W-L352M. Moreover, a control experiment performed in H_2O/D_2O (9:1, v/v) mixture revealed that the substitution of

DOI: 10.1021/acscatal.5b00949
ACS Catal. 2015, 5, 4598−4611

Table 2. Transglycosylation Yields (%) for Reactions Catalyzed by *Tx*Abf and R69H Derivatives[a]

enzyme	XA^3X[b]	A^3XX[b]	(L-Araf) + XA^2X[b]	A^2XX[b]	auto 1[c]	auto 2[c]
*Tx*Abf (pD 5.8)	7.5	11.8	3.3	10.5	6.7	3.2
R69H (pD 7.0)	23.2	25.2	4.9	30.6	3.9	2.2
R69H-L352M (pD 7.0)	20.4	22.2	4.6	27.3	4.7	2.2
R69H-G179F-L352M (pD 7.0)	35.3	17.3	8.4	48.8	2.1	1.6
R69H-N216W-L352M (pD 7.0)	4.6	7.7	8.0	78.6	3.0	7.7
R69H-N216W-L352M (pD 5.8)	0.7	1.2	5.5	71.0	2.3	8.1
R69H-N216W-L352M (H_2O-pH 7.0)	0.9	8.6	6.3	74.6	2.4	7.0
R69H-N216W-L352M (H_2O-pH 5.8)	1.4	1.4	5.4	71.9	2.4	8.1
R69H-N216W-L352M (10% CD_3CN-pD 7.0)	1.7	2	10.5	80.1	2.6	7.8

[a]Maximum yields can be reached at different times explaining the fact that the sum of maximum yields can be superior to 100%. [b]The structures of the transglycosylation products were determined by NMR and were consistent with those previously reported (Figure S1).[29−34] [c]Auto 1 and auto 2 correspond to two regioisomers of self-condensation products.[18]

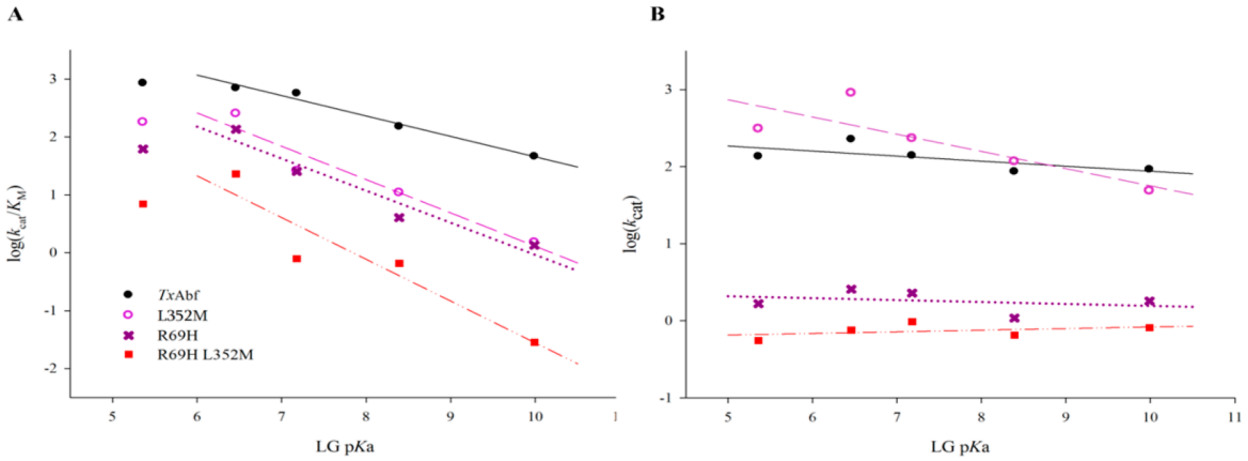

Figure 6. Brønsted plots of the Hammett relationship for the hydrolysis of aryl α-L-arabinofuranosides catalyzed by *Tx*Abf (solid), L352M (dash), R69H (dot), and R69H-L352M (dash-dot-dot). (A) log(k_{cat}/K_M) and (B) log(k_{cat}) are plotted as a function of the pK_a of the LG for a series of LG-α-L-Ara*f*. All the kinetic parameters (Table S7) were derived from triplicate experiments. In Figure 6A, the lowest LG pK_a data point was omitted when establishing the linear data fit (Table S8).

H_2O by D_2O did not affect the H/T partition, because at pH 7.0 and 5.8, equivalent transfer rates and yields were obtained. It is also worth mentioning that the addition of 10% acetonitrile (v/v) in the reaction medium also allowed the suppression of secondary hydrolysis (Figure 5), while procuring a 10% increase in the final yield (Table 2) without changes in the initial H/T partition.

Probing the Mechanisms of Mutant Enzymes. *Hammett−Brønsted Analysis: Transition-State Structure and Rate-Limiting-Step Determination.* To investigate how mutations in subsite −1 (i.e., L352M and R69H) affect the catalytic mechanism, notably in the switch from ground to the first transition state, a Hammett−Brønsted analysis was performed using a series of aryl α-L-arabinofuranosides to probe leaving group (LG) effects (Table S7). Plotting log(k_{cat}/K_M) as a function of the pK_a of the LG (Figure 6A) revealed that while the glycosylation step in reactions catalyzed by *Tx*Abf is relatively insensitive to LG pK_a changes (i.e., $\beta_{LG1} = -0.35$ or -0.28), the mutants R69H, L352M, and R69H-L352M were 1.3 to 2.1-fold more sensitive (Table S8), indicating that these mutants are characterized by modifications in the transition state at the glycosylation step. Moreover, because the catalytic constant ($k_{cat} = k_2.k_3/(k_2 + k_3)$) reflects the rate-limiting step, a plot of log(k_{cat}) as a function of LG pK_a (Figure 6B) was used to reveal whether the LG (released during glycosylation) is involved in this step or not, with the latter outcome implying that deglycosylation is the rate-limiting step. This investigation demonstrated that for most of the mutants and parental *Tx*Abflog(k_{cat}) was rather insensitive to LG pK_a changes, with values of β_{LG2} being close to zero for a wide range of pK_a values up to pK_a = 9.99. Therefore, it was concluded that reactions catalyzed by *Tx*Abf, R69H and R69H-L352M are characterized by a rate-limiting deglycosylation (k_3) step, which is consistent with previous results obtained for other Abfs.[38,39] The only exception to this was L352M, which displayed a slight dependence of k_{cat} on LG pK_a ($\beta_{LG2} = -0.22$). Taken together with the previous observation, this result most likely indicates that this mutation strongly affects the glycosylation step, as suggested by the increase in the K_M value. It is noteworthy that when log(k_{cat}/K_M) was plotted as a function of LG pK_a evolution, the linearity of the different data sets was poor, mainly because of the two lowest LG pK_a points. In this respect, it is pertinent to note that the electron-withdrawing character of the LG might not be the only parameter influencing the glycosylation step. While diffusion-related phenomena are unlikely to exert any influence ($\sim 10^5$ $s^{-1}\cdot mM^{-1} \gg k_{cat}/K_M$),[40] steric hindrances may well affect the efficiency of this catalytic step. It is noteworthy that similar Brønsted profiles have been observed for other glycosidases,[40−42] and that there is no rational or objective reason to consider spurious data points such as those obtained for NCP or 3,4-dNP.

Probing Solvent Kinetic Isotope Effects and the Role of Water. At the deglycosylation step, hydrolysis occurs when water

DOI: 10.1021/acscatal.5b00949
ACS Catal. 2015, 5, 4598−4611

acts as an acceptor, launching a nucleophilic attack on the anomeric carbon of the glycosyl-enzyme (Figures 1 and 2B). This catalytic substep is concomitant with a second substep that involves covalent bond breaking and thus the decomposition of the β-L-Araf-*Tx*Abf intermediate. Accounting for the fact that *Tx*Abf and mutants thereof are deficient in the deglycosylation step and that the reactivity of NCP-α-L-Araf is sufficient to correlate apparent reaction rate to this step, it was assumed that the solvent kinetic isotope effects (sKIE) approach could be used to dissect deglycosylation, providing details on the water-mediated substep. To achieve this, reactions were performed in which H_2O was replaced to different extents by D_2O (Figure S11). Overall, no major changes in relative sKIE were observed, except for L352M, which was less sensitive to D_2O/H_2O exchange than *Tx*Abf. This indicates that in all cases, water nucleophilic attack *per se* is not a critical substep in this enzyme system.

Nevertheless, an absolute sKIE effect was observed (80% residual activity), implying that H_2O to D_2O exchange does affect global catalytic efficiency, probably through modified protein dynamics or solvation,[43] as suggested by the exponential-like curve.[44]

Investigating the Ionization State of Catalytic Residues. The pH-dependency of k_{cat}/K_M was investigated in order to access the apparent pK_a values of the two catalytic residues of the *apo*-enzyme (Figure S12). The presence of R69H and L352 M in mutants was correlated with significant shifts (0.7 to 1.2 units) in the apparent pK_a value of the nucleophile E298, although the ionization state of the acid/base E176 remained globally unaffected (Table S9). Nevertheless, when R69H was present as a single mutation, the basic limb of the pH profile displayed an unusual tail, which is characteristic of major ionization state modifications.[26]

DISCUSSION

Thus, far, probably the most reproducible strategy to convert hydrolytic GHs into artificial TGs is the glycosynthase approach, which calls for the use of highly reactive glycoside donors and hydrolytically impotent (i.e., mutation of the catalytic nucleophile) mutant enzymes.[15,16] Beyond this, no rational strategies for the conversion of GHs into "true" TGs are currently known. This is primarily due to the fact that it has proved very difficult to understand how natural evolutionary processes have furnished for example both transglycosylating and hydrolytic XTHs, or trans-sialidase/sialidase pairs, no doubt because this involves very subtle modifications of the molecular determinants, which thus far have not been unequivocally identified.[13,45,46] In the absence of clear protein engineering guidelines, researchers have tackled the challenge using *in vitro* molecular evolution techniques,[35,47,48] which have provided some interesting results. Nevertheless, these studies have fallen short of a comprehensive elucidation of the mechanisms that have driven the observed GH to TG transition.

In the area of furanose chemistry, little attention has been focused on the development of furanose-acting transglycosylases[18,49,50] despite the fact that the synthesis of furanose-based compounds figures among the more challenging aspects in synthetic chemistry. Moreover, to our knowledge, the glycosynthase approach has not yet been successfully applied to furanosidases, probably because of the difficulty to obtain stable but sufficiently reactive furanoside donor substrates. For this reason and because of our extensive knowledge of *Tx*Abf, a rather robust, well-characterized α-L-arabinofuranosidase from *Thermobacillus xylanyliticus* that already displays some ability to catalyze glycosynthetic reactions, we set out to create a *bona fide* transarabinofuranosylase using a combination of protein engineering strategies: random, *in silico*-driven, and site-saturation mutagenesis.

R69, a Conserved Residue in Clan GH-A and a Possible H/T Modulator. Screening of the randomly mutated library created in this study using L352M as the parental template was performed using a previously described strategy, which identifies hydrolytically impaired mutants. Although rather simplistic, this approach is straightforward and has already proved to be efficient for the engineering of transglycosylase activity into a GH1 β-glycosidase.[35] In a second step, the activity of the selected mutants was measured in the presence of xylotriose, which can act as an acceptor, but also as an inhibitor for *Tx*Abf (Figure 3). This provided the means to select mutants that were either no longer inhibited by xylotriose and/or that displayed improved transglycosylation, taking into account the fact that in the latter case, the rate enhancements observed in the presence of xylotriose were underestimations of the actual transglycosylation improvements, since the number of available active sites (i.e., uninhibited fraction) is inferior to that in the acceptor-free reaction.

Overall, the two-stage screening strategy pinpointed the mutation R69H. Interestingly, R69 is totally conserved among GH51 Abfs (Table S3) and is among the eight key residues that define clan GH-A,[51] which is composed of 19 GH families. Beyond sequence conservation, the spatial location of R69 is also significant, because its side chain points toward the nucleophile residue, and lies within H-bonding distance of the latter (Figure S13). Consequently, it is plausible that the substitution of the equivalent arginine in any member of GH-A could lead to a similar modification of the H/T partition and thus a similar phenotype. Indeed, this appears to be the case, because mutation of R75 in the β-glucosidase from *Thermus thermophilus* (GH-1) has been shown to procure a transglycosylase phenotype.[46]

To better understand how the mutation of R69 favors transglycosylation, it is important to recall that the R69H mutation led to a drastic decrease in k_{cat} and (consequently) k_{cat}/K_M, reflecting both slower deglycosylation and glycosylation steps, respectively. Moreover, the K_M value was lower, suggesting that the covalent glycosyl-enzyme intermediate was subject to accumulation. Taken together, these results are consistent with increased energy barriers for the transition states (TS) that are involved in each of the steps. One explanation for these effects is the loss of a hydrogen bond linking the guanidinium group (pK_a ~ 12.5) of R69 to the carboxyl oxygen of the catalytic nucleophile E298. One would expect this modification to alter the electron displacement system (Figure 2B) and, in particular, affect the ionization state of E298, which is indeed the case, because the pK_a of E298 in the mutant R69H was increased.

It is known that along the double-displacement mechanism, pK_a cycling occurs,[52] with the nucleophile (E298) being negatively charged at the beginning of the reaction and the acid/base (E176) protonated. In *Tx*Abf, this is possible because the acid/base catalyst (E176) displays an apparent pK_a ≈7.5, which is far higher than the pK_a value of a free glutamic acid (~4.5). This high pK_a is probably generated by charge-like repulsion between E176 and its close nucleophilic neighbor, E298, such interactions being necessary to avoid unfavorable Coulombic energetics.[52] Regarding the nucleophile catalyst, the study of the GH1 β-glycosidase from *Spodoptera frugiperda* has revealed that the negative ionization state of its nucleophile

DOI: 10.1021/acscatal.5b00949
ACS Catal. 2015, 5, 4598−4611

catalyst, E399, is stabilized through hydrogen bonding to Y331 and R97, which significantly are equivalent to Y242 and R69 in *Tx*Abf.[53] Overall, these observations support the hypothesis that the altered H/T partition that characterizes R69H is the result of modifications to the nucleophile's ability to attack the anomeric carbon, rather than a direct alteration of the efficiency of the catalytic acid/base. Interestingly, according to our data (not shown), when Y242, a residue that also figures among the eight key residues of GH-A (Figure 2), is substituted by phenylalanine, a phenotype (i.e., decreased H/T ratio) similar to that of R69H is observed. This is unsurprising, because Y242 also interacts with E298 and probably contributes to the definition of its operational charge.

It is now well-recognized that a species having oxocarbenium ion-like character is formed during TS of deglycosylation and that, at least in the case of retaining β-glycosidases, a partial positive charge is developed on the anomeric carbon,[54−56] the latter feature being important for catalysis because the incoming acceptor reacts with this species.[45,57] Therefore, the development of a charge of appropriate magnitude is critical and no doubt facilitates water-mediated deglycosylation.

In this case, although water activation is a required feature, it is likely that there is no need for any energetic contribution from the water molecule itself. Indeed, this is consistent with the conclusions of recent *in silico* analyses performed on other GHs, which indicate that the deglycosylation step is highly dissociative, meaning that the covalent bond that links the enzyme nucleophile to the anomeric carbon of the sugar moiety is almost broken when it is replaced by a bond with water.[58] In the light of these mechanistic details, it appears probable that the mutation R69H provokes a charge modification that impacts on TS, reducing the efficiency of water-mediated deglycosylation.

The Hammett−Brønsted analysis revealed that *Tx*Abf and most of the mutants are characterized by a rate-limiting deglycosylation step for a large range of substrates, an observation that is consistent with data collected for other Abfs[38,39] but different to those collected for glycopyranosidases.[40−42,59,60] For the latter, the Brønsted plot of $\log(k_{cat})$ is usually characterized by a concave breakdown for LGs whose pK_a values are above 8, this transition being indicative of a change in the rate-limiting step (from deglycosylation to glycosylation). Accordingly, for *Tx*Abf, and more generally furanoside hydrolases, it is possible that this difference is linked to the ring strain of furanoside substrates,[61] which makes the decomposition of the glycosyl-enzyme complex (i.e., deglycosylation) more energy demanding than its creation (i.e., glycosylation).

Taken together, the fact that deglycosylation is rate-limiting in *Tx*Abf and mutants thereof, irrespective of the LG, the observation that k_{cat} is strongly decreased in R69H-containing mutant, and the absence of relative changes in sKIE all argue in favor of a highly impaired covalent bond-breaking (deglycosylation) substep in the R69H-containing mutants. However, if one also considers the rather low dependency of k_{cat}/K_M on LG pK_a values, it is also possible to deduce that only a small negative charge is developed on the interglycosidic oxygen at TS of the glycosylation step, which implies that either acid/base protonation is strong enough to compensate for the electronic character of the LG,[62,63] or that during glycosylation the major contribution comes from the catalytic nucleophile, which provides a strong "nucleophilic push" toward the anomeric carbon. In this respect, the more negative β_{LG1} values measured for the mutants containing R69H and/or L352 M provide further evidence for modifications of charge distribution within the TS, along the axis [nucleophile E298 ↔ anomeric carbon ↔ interglycosidic oxygen]. Overall, the kinetics and sKIE data presented in this study point to the fact that the mutations R69H and L352M, disrupt both covalent glycosyl-enzyme bond formation and decomposition and that this is caused by changes in the distribution of electronic charge.

Key Factors That Transform GHs into TGs. *Donor Subsite Mutations Undermine Enzyme Activity but Are Necessary To Counter Water Activity.* From a conceptual standpoint, it is easy to imagine how mutations in the acceptor subsite(s) of GHs could promote the acquisition of transglycosylation ability, by increasing the recognition of the incoming sugar moiety. However, it is much less obvious to casually rationalize the postulate that donor subsite mutations are a prerequisite for the conversion of a GH into a TG, especially in the light of our data that clearly demonstrate that such mutations severely reduce enzyme activity. Nevertheless, the mutation of donor subsite determinants, especially highly conserved residues, has recently been proposed as a semirational strategy to improve the transglycosylation ability of several GHs.[46,64] To better understand why this might be, it is pertinent to recall that GHs generally operate in aqueous environments, dominated by the presence of water (at a concentration of 55 M). Therefore, it is clear that it is imperative for TGs to somehow avoid water-mediated deglycosylation, with the increased lifetime of glycosyl-enzyme intermediates being an outward sign of this.[65] In this study, we have shown that although R69H drastically reduced activity, it had a very positive impact on the H/T ratio. Transglycosylation was clearly favored and water-mediated deglycosylation was reduced, thus diminishing hydrolysis (Figure S14). However, R69H did not eliminate secondary hydrolysis, a reaction that procures products that can no longer act as substrates for further transglycosylation (Figure 1). To achieve this, it was necessary to combine R69H with a second subsite −1 mutation, L352M. Clearly, the introduction of L352 M affected the glycosylation step, a fact revealed by the marked sensitivity of L352M-containing mutants to LG pK_a variations (β_{LG1}) and the very high K_M values measured on LG-α-L-Ara*f*. In this respect, it is noteworthy that, compared to *p*NP (pK_a = 7.18), the xylotriosyl moiety of the transglycosylation products displays much lower leaving group ability (pK_a of glycosidic hydroxyl ∼12), which might explain the reduced ability of L352M-containing mutants to hydrolyze the transglycosylation products.

Acceptor Subsite Modifications Can Produce Different Effects. In this work, two acceptor subsite mutations contributed to the successful creation of transarabinofuranosylases. The first one G179F, located in subsite +1, was selected using an *in silico* approach that employed an algorithm that identifies single mutations that can procure increased binding for a given acceptor. Whereas the introduction of G179F into the double mutant R69H-L352M did not affect the transfer rate, it clearly altered secondary hydrolysis, although the mechanism has yet to be clarified. Nevertheless, it is highly probable that the G179F procures increased hydrophobicity in subsite +1 and a stacking interaction with *p*NP, thus specifically increasing the affinity of the mutant enzyme for *p*NP-α-L-Ara*f*. The implication of this modification is that the donor is probably better recognized compared to the transglycosylation products, and thus, secondary hydrolysis is postponed.

Regarding N216W, when present as a single mutation this subsite +2 mutation only modestly increases the transfer rate and diverts activity away from the formation of (1→3) linkages, while alleviating xylotriose inhibition. Therefore, it is probable

DOI: 10.1021/acscatal.5b00949
ACS Catal. 2015, 5, 4598−4611

that N216W affects both acceptor positioning and affinity. Additionally, as suggested by its nonsaturating acceptor dose−response relationship (Figure 3), the triple mutant R69H-N216W-L352M may reveal the acceptor-activation behavior that R69H-L352M should display without acceptor inhibition, which restrains the apparent acceptor-mediated activity enhancement.

It is noteworthy that the overall transglycosylation yields of the single mutants G179F and N216W remained low, which clearly demonstrates that the modification of acceptor subsites alone is insufficient to confer good transglycosylase activity to *Tx*Abf. However, when the beneficial effects of these mutations were combined with the crippling effects of R69H-L352M, it is significant that almost perfect transfuranosylases were obtained (Figure 7).

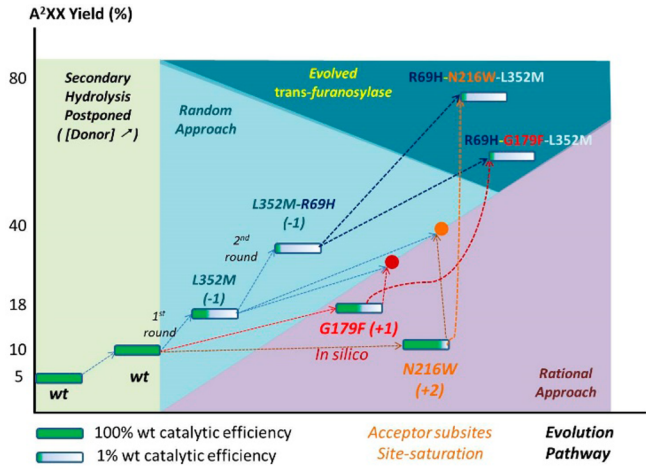

Figure 7. Iterative pathway that allowed the conversion of *Tx*Abf into non-Leloir transarabinofuranosylases. A subtle combination of random, semirational, and *in silico* approaches was used to reach this goal.

Toward an Understanding of the Evolutionary Emergence of TGs. Numerous structural studies, including the one performed on *Tx*Abf,[36] have revealed that *exo*-acting GHs are characterized by extensive enzyme−substrate interaction networks in the donor subsite. Consequently, reactions catalyzed by *exo*-acting GHs are characterized by strong stabilization of the TS (i.e., lowering of energy barriers), which usually results in quite high catalytic efficiencies (k_{cat}/K_M values), linked to a fast glycosylation step, and reasonably efficient (albeit slower) water-mediated deglycosylation. The efficiency of the latter step is underpinned by the fact that the vast majority of the energy required to overcome the TS is procured by donor subsite interactions (Figure S14). This last point is vital to understand the preponderant water-mediated deglycosylation in hydrolytic GHs operating in aqueous media. Nevertheless, despite the overwhelming presence of water, *exo*-acting GHs often display some ability to perform transglycosylation (up to 12% yields for *Tx*Abf regarding the main product and sometimes more for other *exo*-GHs),[66] which is consistent with the fact that acceptor sugars can lower the TS2 energy level at deglycosylation step (Figures S14 and S15). Therefore, acceptor subsite mutations that improve enzyme-(acceptor) substrate interactions can further exacerbate the T/H partition and thus increase transglycosylation yields. When coupled to other mutations that deprive water-mediated deglycosylation of much of the energy that is required to overcome the TS (i.e., ones that perturb donor subsite interactions), potent TGs are produced.

In a recent review, we detailed the ways in which TGs and GHs differ and provided some insight into how we believe Nature has provided these two different activities using a common catalytic mechanism and a whole range of protein scaffolds.[9] Overall, it appears likely that natural evolutionary processes have resulted in a trade-off that inevitably links good transglycosylation to poor transition states and low overall activity, this being the only efficient way to counter the overwhelming competition from water molecules. Consistent with this, we observe that the overall TGs that have so far been thoroughly characterized can indeed be considered catalytically impaired enzymes.[67−69]

CONCLUSION AND PERSPECTIVES

We believe that the enzymes described in this work can be legitimately designated as non-Leloir transfuranosylases (up to 80% yield of the main product, slight and controllable residual hydrolysis). Therefore, to our knowledge, this is the first example of the *in vitro* creation of such enzymes. In this respect, the work described herein should have far-reaching consequences, notably because it provides precious tools for furanose chemistry and a number of critical elements for the elaboration of a more generic protein engineering strategy that can be applied to GHs. Concerning the perspectives for furanose chemistry, it is noteworthy that *Tx*Abf and other L-arabinofuranosidases display the ability to transfer D-galactofuranosyl moieties onto acceptors. D-Galactofuranose is a rare sugar of considerable importance, because it is widespread in human microbial pathogens.[70] Therefore, the enzymes developed in this work could be useful for the synthesis of medically relevant compounds.

Regarding the protein engineering strategy, it is noteworthy that random mutagenesis coupled to a quite simple screening method appears to be suitable to isolate mutants that are hydrolytically crippled, although in the future it may be even more efficient to directly mutate residues that are likely to form hydrogen bonds with the catalytic nucleophile in the substrate donor site (beginning with homologues of *Tx*Abf R69) and/or highly conserved around the donor subsite (−1). These could be combined with direct mutation(s) that increase the affinity or the positioning of the acceptor, predicting hot-spots using *in silico* approaches such as the one described herein. Overall, we believe that the lessons learned in this work provide the basis for a general GH engineering route that should allow the successful improvement of transglycosylase activity in other *exo*-acting GHs.

ASSOCIATED CONTENT

Supporting Information

The Supporting Information is available free of charge on the ACS Publications website at DOI: 10.1021/acscatal.5b00949.

Experimental information pertaining to the synthesis of aryl α-L-arabinofuranoside donors and *in silico* calculations, as well as further details on random mutagenesis analysis, screening methods, structure/function relationships, conservation of targeted residues, regioselectivity and biochemical data (PDF)

AUTHOR INFORMATION

Corresponding Authors

*E-mail: michael.odonohue@insa-toulouse.fr.
*E-mail: regis.faure@insa-toulouse.fr.

Notes

The authors declare no competing financial interest.

DOI: 10.1021/acscatal.5b00949
ACS Catal. 2015, 5, 4598−4611

■ ACKNOWLEDGMENTS

The PhD fellowship of B.B. was supported by the Institut National de la Recherche Agronomique (INRA) [CJS]. The NMR work carried out in this work at the Laboratory for BioSystems & Process Engineering (Toulouse, France) was performed with the equipment of MetaToul (Metabolomics & Fluxomics Facitilies, Toulouse, France, www.metatoul.fr). MetaToul is part of the national infrastructure MetaboHUB (The French National infrastructure for metabolomics and fluxomics, www.metabohub.fr) and is supported by grants from the Région Midi-Pyrénées, the European Regional Development Fund, SICOVAL, IBiSa-France, the Centre National de la Recherche Scientifique (CNRS) and INRA. We thank the ICEO facility dedicated to enzyme screening and discovery and part of the Integrated Screening Platform of Toulouse (PICT, IBiSA) for providing access to the TECAN liquid handling equipment. Contributions from X.B. and A.P. were partially supported by grant BIO2013-49022-C2-1-R from MINECO, Spain.

■ ABBREVIATIONS

Abfs, α-L-arabinofuranosidases; L-Ara*f*, L-arabinofuranosyl; AXOS, arabinoxylo-oligosaccharides; A^2XX, α-L-Ara*f*-(1→2)-β-D-Xyl*p*-(1→4)-β-D-Xyl*p*-(1→4)-D-Xyl*p*; A^3XX, α-L-Ara*f*-(1→3)-β-D-Xyl*p*-(1→4)-β-D-Xyl*p*-(1→4)-D-Xyl*p*; 3,4-dNP, 3,4-dinitrophenol; GH, glycoside hydrolase; GT, glycosyltransferase; LG, leaving group; NCP, 2-nitro-4-chlorophenol; 3-NP, 3-nitrophenol; Ph, phenol; *p*NP, 4-nitrophenol; *p*NP-α-L-Ara*f*, 4-nitrophenyl α-L-arabinofuranoside; r-GH, retaining GH; sKIE, solvent kinetic isotope effects; *Tx*Abf, α-L-arabinofuranosidase from *Thermobacillus xylanilyticus*; H/T, hydrolysis/transglycosylation ratio; TG, non-Leloir transglycosylase; TS, transition state; X, donor substrate conversion rate; X-α-L-Ara*f*, 5-bromo-4-chloro-3-indolyl α-L-arabinofuranoside; XA^2X, β-D-Xyl*p*-(1→4)-[α-L-Ara*f*-(1→2)]-β-D-Xyl*p*-(1→4)-D-Xyl*p*; XA^3X, β-D-Xyl*p*-(1→4)-[α-L-Ara*f*-(1→3)]-β-D-Xyl*p*-(1→4)-D-Xyl*p*; XOS, xylo-oligosaccharides; D-Xyl*p*, D-xylopyranosyl; Y, yield.

■ REFERENCES

(1) Lowary, T. *Curr. Opin. Chem. Biol.* **2003**, *7*, 749−756.
(2) Peltier, P.; Euzen, R.; Daniellou, R.; Nugier-Chauvin, C.; Ferrières, V. *Carbohydr. Res.* **2008**, *343*, 1897−1923.
(3) Fauré, R.; Saura-Valls, M.; Brumer, H.; Planas, A.; Cottaz, S.; Driguez, H. *J. Org. Chem.* **2006**, *71*, 5151−5161.
(4) Champion, E.; André, I.; Moulis, C.; Boutet, J.; Descroix, K.; Morel, S.; Monsan, P.; Mulard, L. A.; Remaud-Siméon, M. *J. Am. Chem. Soc.* **2009**, *131*, 7379−7389.
(5) Wang, L.-X.; Huang, W. *Curr. Opin. Chem. Biol.* **2009**, *13*, 592−600.
(6) Wang, Z.; Chinoy, Z. S.; Ambre, S. G.; Peng, W.; McBride, R.; de Vries, R. P.; Glushka, J.; Paulson, J. C.; Boons, G.-J. *Science* **2013**, *341*, 379−383.
(7) Koshland, D. E., Jr. *Biol. Rev.* **1953**, *28*, 416−436.
(8) Lombard, V.; Golaconda Ramulu, H.; Drula, E.; Coutinho, P. M.; Henrissat, B. *Nucleic Acids Res.* **2014**, *42*, D490−D495.
(9) Bissaro, B.; Monsan, P.; Fauré, R.; O'Donohue, M. *Biochem. J.* **2015**, *467*, 17−35.
(10) Street, I. P.; Kempton, J. B.; Withers, S. G. *Biochemistry* **1992**, *31*, 9970−9978.
(11) Ducros, V. M.; Tarling, C. A.; Zechel, D. L.; Brzozowski, A. M.; Frandsen, T. P.; von Ossowski, I.; Schülein, M.; Withers, S. G.; Davies, G. J. *Chem. Biol.* **2003**, *10*, 619−628.
(12) Zakariassen, H.; Hansen, M. C.; Jøranli, M.; Eijsink, V. G. H.; Sørlie, M. *Biochemistry* **2011**, *50*, 5693−5703.
(13) Eklöf, J. M.; Shojania, S.; Okon, M.; McIntosh, L. P.; Brumer, H. *J. Biol. Chem.* **2013**, *288*, 15786−15799.
(14) Saburi, W.; Kobayashi, M.; Mori, H.; Okuyama, M.; Kimura, A. *J. Biol. Chem.* **2013**, *288*, 31670−31677.
(15) Mackenzie, L. F.; Wang, Q.; Warren, R. A. J.; Withers, S. G. *J. Am. Chem. Soc.* **1998**, *120*, 5583−5584.
(16) Malet, C.; Planas, A. *FEBS Lett.* **1998**, *440*, 208−212.
(17) Debeche, T.; Cummings, N.; Connerton, I.; Debeire, P.; O'Donohue, M. J. *Appl. Environ. Microbiol.* **2000**, *66*, 1734−1736.
(18) Rémond, C.; Plantier-Royon, R.; Aubry, N.; O'Donohue, M. J. *Carbohydr. Res.* **2005**, *340*, 637−644.
(19) Rémond, C.; Plantier-Royon, R.; Aubry, N.; Maes, E.; Bliard, C.; O'Donohue, M. J. *Carbohydr. Res.* **2004**, *339*, 2019−2025.
(20) Arab-Jaziri, F.; Bissaro, B.; Dion, M.; Saurel, O.; Harrison, D.; Ferreira, F.; Milon, A.; Tellier, C.; Fauré, R.; O'Donohue, M. J. *New Biotechnol.* **2013**, *30*, 536−544.
(21) Arab-Jaziri, F.; Bissaro, B.; Tellier, C.; Dion, M.; Fauré, R.; O'Donohue, M. J. *Carbohydr. Res.* **2015**, *401*, 64−72.
(22) Kelly, M. A.; Sinnott, M. A.; Widdows, D. *Carbohydr. Res.* **1988**, *181*, 262−266.
(23) Bissaro, B.; Saurel, O.; Arab-Jaziri, F.; Saulnier, L.; Milon, A.; Tenkanen, M.; Monsan, P.; O'Donohue, M. J.; Fauré, R. *Biochim. Biophys. Acta, Gen. Subj.* **2014**, *1840*, 626−636.
(24) Patrick, W. M.; Firth, A. E.; Blackburn, J. M. *Protein Eng., Des. Sel.* **2003**, *16*, 451−457.
(25) Joshi, M. D.; Sidhu, G.; Nielsen, J. E.; Brayer, G. D.; Withers, S. G.; McIntosh, L. P. *Biochemistry* **2001**, *40*, 10115−10139.
(26) Bicknell, R.; Knott-Hunziker, V.; Waley, S. G. *Biochem. J.* **1983**, *213*, 61−66.
(27) Glasoe, P. K.; Long, F. A. *J. Phys. Chem.* **1960**, *64*, 188−190.
(28) Gottlieb, H. E.; Kotlyar, V.; Nudelman, A. *J. Org. Chem.* **1997**, *62*, 7512−7515.
(29) Gruppen, H.; Hoffmaann, R. A.; Kormelink, F. J.; Voragen, A. G.; Kamerlin, J. P.; Vliegenthart, J. F. *Carbohydr. Res.* **1992**, *233*, 45−64.
(30) Viëtor, R. J.; Hoffmann, R. A.; Angelino, S. A. G. .; Voragen, A. G. J.; Kamerling, J. P.; Vliegenthart, J. F. G. *Carbohydr. Res.* **1994**, *254*, 245−255.
(31) Ferré, H.; Broberg, A.; Duus, J. O.; Thomsen, K. K. *Eur. J. Biochem.* **2000**, *267*, 6633−6641.
(32) Pastell, H.; Tuomainen, P.; Virkki, L.; Tenkanen, M. *Carbohydr. Res.* **2008**, *343*, 3049−3057.
(33) Pitkänen, L.; Tuomainen, P.; Virkki, L.; Tenkanen, M. *Int. J. Biol. Macromol.* **2011**, *49*, 963−969.
(34) Correia, M. A. S.; Mazumder, K.; Brás, J. L. A.; Firbank, S. J.; Zhu, Y.; Lewis, R. J.; York, W. S.; Fontes, C. M. G. A.; Gilbert, H. J. *J. Biol. Chem.* **2011**, *286*, 22510−22520.
(35) Feng, H.-Y.; Drone, J.; Hoffmann, L.; Tran, V.; Tellier, C.; Rabiller, C.; Dion, M. *J. Biol. Chem.* **2005**, *280*, 37088−37097.
(36) Paës, G.; Skov, L. K.; O'Donohue, M. J.; Rémond, C.; Kastrup, J. S.; Gajhede, M.; Mirza, O. *Biochemistry* **2008**, *47*, 7441−7451.
(37) Fauré, R.; Courtin, C. M.; Delcour, J. A.; Dumon, C.; Faulds, C. B.; Fincher, G. B.; Fort, S.; Fry, S. C.; Halila, S.; Kabel, M. A.; Pouvreau, L.; Quemener, B.; Rivet, A.; Saulnier, L.; Schols, H. A.; Driguez, H.; O'Donohue, M. J. *Aust. J. Chem.* **2009**, *62*, 533−537.
(38) Shallom, D.; Belakhov, V.; Solomon, D.; Shoham, G.; Baasov, T.; Shoham, Y. *J. Biol. Chem.* **2002**, *277*, 43667−43673.
(39) Wan, C.; Chen, W.; Chen, C.; Chang, M.; Lo, L.; Li, Y. *Biochem. J.* **2007**, *401*, 551−558.
(40) Zechel, D. L.; Reid, S. P.; Stoll, D.; Nashiru, O.; Warren, R. A. J.; Withers, S. G. *Biochemistry* **2003**, *42*, 7195−7204.
(41) Bravman, T.; Zolotnitsky, G.; Belakhov, V.; Shoham, G.; Henrissat, B.; Baasov, T.; Shoham, Y. *Biochemistry* **2003**, *42*, 10528−10536.
(42) Kempton, J. B.; Withers, S. G. *Biochemistry* **1992**, *31*, 9961−9969.
(43) Combes, D.; Yoovidhya, T.; Girbal, E.; Willemot, R.-M.; Monsan, P. *Ann. N. Y. Acad. Sci.* **1987**, *501*, 59−62.
(44) Schowen, K. B.; Limbach, H. H.; Denisov, G. S.; Schowen, R. L. *Biochim. Biophys. Acta, Bioenerg.* **2000**, *1458*, 43−62.
(45) Pierdominici-Sottile, G.; Palma, J.; Roitberg, A. E. *Proteins: Struct., Funct., Genet.* **2014**, *82*, 424−435.

DOI: 10.1021/acscatal.5b00949
ACS Catal. 2015, 5, 4598−4611

(46) Teze, D.; Hendrickx, J.; Czjzek, M.; Ropartz, D.; Sanejouand, Y.-H.; Tran, V.; Tellier, C.; Dion, M. *Protein Eng., Des. Sel.* **2014**, *27*, 13−19.
(47) Osanjo, G.; Dion, M.; Drone, J.; Solleux, C.; Tran, V.; Rabiller, C.; Tellier, C. *Biochemistry* **2007**, *46*, 1022−1033.
(48) Placier, G.; Watzlawick, H.; Rabiller, C.; Mattes, R. *Appl. Environ. Microbiol.* **2009**, *75*, 6312−6321.
(49) Almendros, M.; Danalev, D.; François-Heude, M.; Loyer, P.; Legentil, L.; Nugier-Chauvin, C.; Daniellou, R.; Ferrières, V. *Org. Biomol. Chem.* **2011**, *9*, 8371−8378.
(50) Chlubnova, I.; Filipp, D.; Spiwok, V.; Dvorakova, H.; Daniellou, R.; Nugier-Chauvin, C.; Kralova, B.; Ferrières, V. *Org. Biomol. Chem.* **2010**, *8*, 2092−2102.
(51) Durand, P.; Lehn, P.; Callebaut, I.; Fabrega, S.; Henrissat, B.; Mornon, J. P. *Glycobiology* **1997**, *7*, 277−284.
(52) McIntosh, L. P.; Hand, G.; Johnson, P. E.; Joshi, M. D.; Korner, M.; Plesniak, L. A.; Ziser, L.; Wakarchuk, W. W.; Withers, S. G. *Biochemistry* **1996**, *35*, 9958−9966.
(53) Marana, S. R.; Mendonça, L. M. F.; Andrade, E. H. P.; Terra, W. R.; Ferreira, C. *Eur. J. Biochem.* **2003**, *270*, 4866−4875.
(54) Notenboom, V.; Birsan, C.; Nitz, M.; Rose, D. R.; Warren, R. A. J.; Withers, S. G. *Nat. Struct. Biol.* **1998**, *5*, 812−818.
(55) Vocadlo, D. J.; Davies, G. J. *Curr. Opin. Chem. Biol.* **2008**, *12*, 539−555.
(56) Davies, G. J.; Planas, A.; Rovira, C. *Acc. Chem. Res.* **2012**, *45*, 308−316.
(57) Pierdominici-Sottile, G.; Horenstein, N. A.; Roitberg, A. E. *Biochemistry* **2011**, *50*, 10150−10158.
(58) Brás, N. F.; Ramos, M. J.; Fernandes, P. A. *J. Mol. Struct.: THEOCHEM* **2010**, *946*, 125−133.
(59) Tull, D.; Withers, S. G. *Biochemistry* **1994**, *33*, 6363−6370.
(60) Vallmitjana, M.; Ferrer-Navarro, M.; Planell, R.; Abel, M.; Ausín, C.; Querol, E.; Planas, A.; Pérez-Pons, J.-A. *Biochemistry* **2001**, *40*, 5975−5982.
(61) Taha, H. A.; Richards, M. R.; Lowary, T. L. *Chem. Rev.* **2013**, *113*, 1851−1876.
(62) Ly, H. D.; Withers, S. G. *Annu. Rev. Biochem.* **1999**, *68*, 487−522.
(63) Kelly, M. A.; Sinnott, M. L.; Herrchen, M. *Biochem. J.* **1987**, *245*, 843−849.
(64) Teze, D.; Daligault, F.; Ferrières, V.; Sanejouand, Y.-H.; Tellier, C. *Glycobiology* **2015**, *25*, 420−427.
(65) Piens, K.; Fauré, R.; Sundqvist, G.; Baumann, M. J.; Saura-Valls, M.; Teeri, T. T.; Cottaz, S.; Planas, A.; Driguez, H.; Brumer, H. *J. Biol. Chem.* **2008**, *283*, 21864−21872.
(66) Dion, M.; Nisole, A.; Spangenberg, P.; André, C.; Glottin-Fleury, A.; Mattes, R.; Tellier, C.; Rabiller, C. *Glycoconjugate J.* **2001**, *18*, 215−223.
(67) Potocki de Montalk, G.; Remaud-Siméon, M.; Willemot, R. M.; Sarçabal, P.; Planchot, V.; Monsan, P. *FEBS Lett.* **2000**, *471*, 219−223.
(68) Baumann, M. J.; Eklöf, J. M.; Michel, G.; Kallas, A. M.; Teeri, T. T.; Czjzek, M.; Brumer, H. *Plant Cell* **2007**, *19*, 1947−1963.
(69) Ribeirão, M.; Pereira-Chioccola, V. L.; Eichinger, D.; Rodrigues, M. M.; Schenkman, S. *Glycobiology* **1997**, *7*, 1237−1246.
(70) Pedersen, L. L.; Turco, S. J. *Cell. Mol. Life Sci.* **2003**, *60*, 259−266.

DOI: 10.1021/acscatal.5b00949
ACS Catal. 2015, 5, 4598−4611